Chapter 6

SIMULATING THE IN SITU OXIDATIVE TREATMENT OF CHLORINATED ETHYLENES BY POTASSIUM PERMANGANATE

H. Zhang and F. W. Schwartz

Introduction

In recent years, MnO_4^- oxidation of chlorinated ethylenes (PCE, TCE and DCE) has emerged as a potentially useful approach for destroying these compounds in water (Vella and Veronda, 1992; Gates *et al*., 1995; Schnarr *et al*., 1998; Yan and Schwartz, 1998 and 1999). The ability of MnO_4^- to oxidize some organic compounds has been known for a long time. Steward (1965) extensively reviewed the role of $KMnO_4$ in organic reactions. Colthust and Singer (1982) noticed that adding $KMnO_4$ to drinking water reduced the concentration of trihalomethane (THM) precursors. Moreover, the concentration of these humic substances was further reduced in the presence of Ca^{2+} through sorption on manganese dioxide, a product of the oxidation reaction.

Recently, more applied studies have looked at whether $KMnO_4$ could be used in remediating sites contaminated by chlorinated solvents. Schnarr *et al*. (1998) reported the results of laboratory and controlled field experiments using $KMnO_4$ to remediate trichloroethylene and perchloroethylene. West *et al*. (1997) undertook a field demonstration of the *in situ* scheme for source-zone remediation at a DOE facility. Yan and Schwartz (1998, 1999) examined the kinetic behavior of chlorinated ethylenes in reactions with MnO_4^-. Drescher *et al*. (1998) demonstrated that organic matter in the soils exerts a greater competitive demand for MnO_4^- than the NAPL. Pilot tests for treatment of TCE were also performed in unsaturated zones (LaChance *et al*., 1998; McKay *et al*., 1998).

Almost all of the work to date has been concerned with understanding the nature and kinetics of key reactions, and assessing the remedial concept in controlled laboratory and field experiments. There is no published work on numerical models that could be used in the design and evaluation of this scheme under field conditions. However, development of a three-dimensional model is a natural step in the development of this technology. Such a model could help to optimize the engineering designs to reduce the cost and potential adverse side effects.

This paper describes a new computer code (ISCO3D), which was developed to simulate the coupled processes of NAPL dissolution, chemical reactions, and solute mass transport in the *in-situ* oxidization scheme. The code is also capable of simulating key reactions between the aquifer material and MnO_4^- and the kinetic sorption of chemicals, and has been optimized for computational efficiency. The code fills the gap between the laboratory studies and field operations by providing a numerical model capable of assisting with the design of systems and the interpretation of field observations.

The first few sections of this paper will provide numerical framework of the model. The code is demonstrated in applications involving column experiments (Schnarr *et al*., 1998), a test cell experiment (Schnarr *et al*., 1998), and a field demonstration (West *et al*., 1997).

Mathematical Formulation

In the following development of mathematical equations, it is assumed that there exists a zone of residual NAPL or a dissolved plume of chlorinated compounds in the saturated zone. MnO_4^- is injected into an aquifer as an oxidant and assumed to follow some flow path. The MnO_4^- is assumed to react with natural organic carbon and other oxidizable aquifer materials, as well as the dissolved chlorinated compounds in the aqueous phase. With the injection of MnO_4^- into a NAPL zone, the utilization of contaminants in the aqueous phase accelerates the dissolution of the NAPL.

Assuming that the NAPL is immobile and the saturation of the NAPL in the medium is small, the ground-water flow equation can be written as (Bear, 1972; Frind, 1983);

$$\nabla(K\,\nabla h) + Q = S_s \frac{\partial h}{\partial t} \tag{6.1}$$

where **K** is the hydraulic conductivity tensor (L/T), h is the water head (L), Q is the source (L^3/T), t is the time (T), and S_s is the specific storage (L^{-1}).

The mass-transport equation (modified from Bear, 1972; Huyakorn and Pinder, 1983) for mobile species is expressed as;

$$\nabla(nD\nabla c_i) - \nabla(nVc_i) + r_i = \frac{\partial(n\,c_i)}{\partial t} \tag{6.2}$$

where n is porosity, **D** is the dispersion coefficient tensor (L^2T^{-1}), V is the linear groundwater velocity vector (LT^{-1}), c_i is the concentration for species i (ML^{-3}), and r_i is the reaction rate for species i ($ML^{-3}\,T^{-1}$).

Yan and Schwartz (1999) found that the oxidation of PCE, TCE, and three isomers of DCE involved two sequential reactions, illustrated here for TCE;

$$C_2HCl_3 + MnO_4^- \xrightarrow{k_1} I \xrightarrow{k_2} \gamma CA + MnO_2 + 3Cl^- \tag{6.3}$$

where I is a cyclic complex, CA are various carboxylic acids, and k_1, and k_2 are rate constants. Our modeling approach is sufficiently general to accommodate reactions of this kind. We conducted preliminary trials to examine the overall behavior of the various carboxylic acids that formed. Unfortunately, for large multi-dimensional problems, large execution times made

solving this reaction network infeasible. A simplified approach was adopted which abstracted the chemical reactions between MnO_4^- and tetrachloroethene (PCE), trichloroethene (TCE), and dichloethene (DCE), and aquifer material (for example, natural organic carbon) as follows;

(a) PCE;

$$C_2Cl_4 + 2MnO_4^- \Rightarrow 4Cl^- + 2CO_2 + 2MnO_2(s) \quad (6.3)$$

(b) TCE;

$$C_2HCl_3 + 2MnO_4^- \Rightarrow 3Cl^- + 2CO_2 + H^+ + 2MnO_2(s) \quad (6.4)$$

(c) DCE;

$$C_2H_2Cl_2 + 2MnO_4^- \Rightarrow 2Cl^- + 2CO_2 + 2H^+ + 2MnO_2(s) \quad (6.5)$$

(d) Natural Organic Matter;

$$C + MnO_4^- \Rightarrow CO_2 + MnO_2(s) \quad (6.6)$$

(e) Sorption Reaction;

$$C_2Cl_4 \Leftrightarrow C_2Cl_4(s) \quad (6.7)$$

The equations for the oxidation of chlorinated compounds (6.3) through (6.5) have a form that is similar to that as illustrated here for TCE;

$$\frac{d(TCE)}{dt} = -k_{TCE}(TCE)(MnO_4^-) \quad (6.8)$$

where ( ) indicate concentrations and k_{TCE} is the rate constant (s^{-1}) for the oxidation of TCE. The values for these constants come from kinetic batch experiments (Table 6.1). In these experiments, initial TCE concentration varied from 0.031 to 0.083 mM while initial MnO_4^- concentration changed from 0.37 to 1.2 mM.

Table 6.1. Kinetic rate constants for PCE, TCE, and DCE oxidation by MnO_4^-.

Chlorinated Ethylenes	k ($M^{-1}s^{-1}$)
PCE	0.045
TCE	0.65
Cis-DCE	0.92
Trans-DCE	30
1,1-DCE	2.38
OAM	450

The reaction rate data indicate that it is much easier to oxidize DCE with MnO_4^- than TCE. Similarly, the reaction rate between TCE and MnO_4^- is faster than that between PCE and MnO_4^-.

Equation (6.6) represents the oxidization of aquifer materials by MnO_4^- as a single reaction. In reality, MnO_4^- reacts with a variety of oxidizable species in solid and dissolved phases. It is assumed that the oxidation of aquifer materials by MnO_4^- has this rate law;

$$\frac{d(OAM)}{dt} = -k_{OAM}(OAM)(MnO_4^-) \quad (6.9)$$

where (OAM) is the concentration of oxidizable aquifer material and k_{OAM} is the pseudo rate constant. Our simplified treatment is in keeping with the limited information related to MnO_4^- consumption by aquifer materials. There is little published information as to values of k_{OAM}. The column experiments by Schnarr *et al.* (1998) show the breakthrough of MnO_4^- to be considerably delayed as a consequence of competitive utilization by the oxidation of the porous medium. These results indicate that the reaction between the MnO_4^- and the oxidizable aquifer material is much faster as compared to contaminant transport time. In the simulations that follow, we assume k_{OAM} >> rate constants for the chlorinated compounds. In effect, this assumption produces an MnO_4^- transport velocity that depends on (OAM).

Equation (6.7) is a kinetic sorption/mass transfer equation for PCE. Kinetic sorption of other compounds can be expressed in a similar way. There is some evidence from field experiments that a kinetic approach is appropriate. Roberts *et al.* (1986) showed that the retardation factor increases from 2.7 at 15 days to 5.9 at 650 day for PCE transport in the Borden aquifer. The increase of retardation factor with time is one of the indicators of kinetic sorption (Zhang *et al.*, 1998).

The chemical reactions are included in (6.2) through the source term. All of the transport equations are written in terms of the concentration, although provision is made in the code to provide mass-law expressions in terms of activity.

Kinetic Dissolution Model for NAPLs

The rate of organic dissolution can be described by;

$$n\frac{dc_i}{dt} = k_{Ni}(c_{Si} - c_i) \quad (6.10)$$

where c_i is the aqueous concentration corresponding to NAPL species i (ML^{-3}), k_{Ni} is the mass transfer coefficient (T^{-1}), and c_{Si} is the equilibrium concentration with pure organic liquid or solubility of species i (Pfannkuch, 1984; Sleep and Sykes, 1989; and Miller *et al.*, 1990). Some investigators (Sleep and Sykes, 1989) used a lumped mass transfer coefficient in their sensitivity analysis for mass transfer between phases. Others (Pfannkuch,

1984; Miller *et al*., 1990; and Powers *et al*., 1992) used correlation expressions to relate the mass transfer coefficient to Reynolds and Schmidt numbers, and other physical parameters. The correlation expressions were chosen in this study because they are more closely related to ground-water flow and properties of NAPLs. To summarize these correlation expressions, several dimensionless numbers need to be defined. The Reynolds number is;

$$Re = \frac{v_w \rho_w d_{50}}{\mu_w} \tag{6.11}$$

and the Sherwood number is;

$$Sh = \frac{k_{Ni} d_{50}^2}{D_m} \tag{6.12}$$

where v_W is the linear groundwater velocity (LT^{-1}), μ_W is the density of aqueous phase fluid, μ_W is the viscosity of the aqueous phase fluid ($ML^{-1}T^{-1}$), d_i means i% of the particles smaller than d_i (L), and D_m is the aqueous molecular diffusion coefficient of the NAPL (L^2T^{-1}). The Sherwood number relates mass transfer coefficient to particle diameter and molecular diffusion coefficient. Several empirical expressions were determined from column experiments (Miller *et al*., 1990; Imhoff *et al*., 1994; and Powers *et al*., 1994). Although these expressions are all useful to determine mass transfer coefficient, a simplified relationship adopted in this study matched better with simulations.

$$Sh = \alpha' Re^{\beta_1'} S_N^{\beta_2'} \tag{6.13}$$

where α', β_1', and β_2' are fitting parameters, respectively, S_N is the NAPL saturation, and Re is the Reynolds number. Comparison between the equation (6.13) and models formulated by other researchers are shown in Table 6.2. The variables δ, U_i, and S_{N0} in the Power's model are the normalized grain size, the uniformity of the grains, the original saturation of NAPL, respectively. The variable X in the Imhoff's model is the distance from the flux entry point of a column to the measurement point in the column. The equation (6.13) is a generic expression of the models proposed by Miller *et al*. (1990), Imhoff *et al*. (1994), and Powers *et al*. (1994). The original models by Imhoff *et al*. (1994), Power *et al*. (1994), and Miller *et al*. (1990) were tied to constant coefficients α', β_1', and β_2' for their experiments. These constant coefficients are different in the three models, and are functions of the grain size, grain shape, grain packing, porosity of media, and other factors. Fitting α', β_1', and β_2' to some values in our simulations provides equation (6.13) the flexibility to reflect the heterogeneity of geological materials in a variety of conditions.

Numerical Formulation

Solution Procedures for Coupled Nonlinear Equations

This section describes the approach to solve the problem of reactive mass transport. To facilitate the description, consider the transport equation expressed in operator notation as;

$$\frac{\partial c_i}{\partial t} + L(c_i) = r_i \tag{6.14}$$

where

$$L = \nabla \bullet (n\, v - n\, D \nabla) \tag{6.15}$$

In general, there are three approaches to couple transport equations with chemical reactions: global implicit, sequential iterative and sequential non-iterative (Steefel and MacQuarrie, 1996). The global implicit approach solves the concentrations of all species at all nodes using Newton or other non-linear procedures. The global implicit approach may be feasible for multiple species mass transport in one dimension, but is considered costly in terms of computational time and computer memory for 3-D problems (Yeh and Tripathi, 1989). The sequential iteration approach accomplishes coupling by iterating between the reaction and transport terms and may not converge in some cases. The sequential non-iterative approach solves the transport and reaction equations in separate steps but may result in errors for a large time step (Valocchin and Malmstead, 1992). To improve the accuracy of reactive transport in the sequential non-iterative approach, a time-centered method, Strang splitting, was used to couple the physical transport and chemical reactions. Strang splitting is similar to the alternating operator-

Table 6.2. Selected dissolution models by different researchers.

Current model	Power's model	Imhoff's model	Miller's model
$\alpha' Re^{\beta_1'} S_N^{\beta_2'}$	$4.13 Re^{0.598} \delta^{0.673} U_i^{0.369} \left(\frac{S_N}{S_{N0}}\right)^{0.5-1.0}$	$340 Re^{0.71} \left(\frac{d_{50}}{X}\right)^{0.31} (nS_N)^{0.87}$	$425 Re^{0.75} (nS_N)^{0.60}$
α'	$\frac{4.13 \delta^{0.673} U_i^{0.369}}{S_{N0}^{0.5-1.0}}$	$340 \left(\frac{d_{50}}{X}\right)^{0.31} (n)^{0.87}$	$425 (n)^{0.60}$
β_1'	0.598	0.71	0.75
β_2'	0.5-1.0	0.87	0.60

splitting scheme proposed by Valocchin and Malmstead (1992) to reduce mass balance errors. In the Strang-splitting approach, changes in solute mass are calculated in two transport time steps and one reaction time step. The solution steps may be summarized as follows (modified from Zysset *et al*., 1994):

(1) Specify initial and boundary conditions.

(2) Solve the ground-water flow equation.

(3) Solve the mass transport equation (6.2) for each species without reaction for half a time step, or ;

$$\frac{c_i^T - c_i^k}{\Delta t/2} + L(c_i) = 0 \tag{6.16}$$

where c_i^T is the concentration at time step k+1/2, Δt is the time step size in the numerical solution of the advection-dispersion equation, and c_i^k is the concentration of species i at time step k.

(4) Calculate the dissolution of NAPLs according to equation (6.10) with an equation of this form;

$$\frac{c_i^D - c_i^T}{\Delta t} = k_{Ni}(c_{Si} - c_i^T) \tag{6.17}$$

where c_i^D is the concentration of species i after a dissolution step for the current time step. The concentration of species without a corresponding NAPL phase does not change during the dissolution step. The size of the time step cannot exceed the inverse of mass transfer coefficient k_{Ni}, maintaining the maximum concentration at or below the aqueous solubility of the species. Mathematically, this constraint is expressed as;

$$\Delta t \le \frac{1}{k_{Ni}} \tag{6.18}$$

The time step size is also constrained by the NAPL available for dissolution in each time step. This constraint has the following form;

$$\Delta t \le \frac{S\rho_N}{k_{Ni}(c_{Si} - c_i^T)} \tag{6.19}$$

where ρ_N is the density of the NAPL, and S is the saturation of the NAPL at a node.

(5) The next step is to solve the reaction equation for each species without transport term, solving a set of equations that have this general form;

$$\frac{c_i^R - c_i^D}{\Delta t} = r_i(c_1, c_2, ..., c_n) \tag{6.20}$$

where c_i^R is the concentration of species i after a reaction step.

(6) Solve the following form of the transport equation (6.2) for each species without reaction for half a time-step size;

$$\frac{c_i^{k+1} - c_i^R}{\Delta t/2} + L(c_i) = 0 \tag{6.20}$$

where c_i^{k+1} is the concentration at time step k+1.

(7) Depending upon the accuracy requirement for the problem, a non-iterative or iterative procedure may be selected for the operator-splitting algorithm. In the iterative procedure, once convergence of the solutions in this step is achieved, you proceed to the next time. For a non-iterative option, go to the next time step.

In this study, the size of the time steps is kept reasonable to make the Strang-splitting approach accurate and efficient for the reactive transport simulation. The numerical procedures for solving mass transport equations (6.16) and (6.21) and reaction equation (20) will be discussed in the following sections.

Finite-Volume Discretization of Flow and Transport Equations

The flow and transport equations were discretized by the finite-volume method. In this discretization scheme, the simulation domain consists of a finite number of control volumes. Each control volume maintains its mass balance (Letniowski and Forsyth, 1991). Flow-balance equations can be obtained by integrating equation (6.1) over a control volume;

$$\iiint_{\Delta V} \nabla(K\nabla h)dxdydz + \iiint_{\Delta V} Q dxdydz = \iiint_{\Delta V} S_s \frac{\partial h}{\partial t} dxdydz \tag{6.22}$$

Similarly, solute mass balance equations can be written as;

$$\iiint_{\Delta V} [\nabla(nD\nabla c_i) - \nabla(nVc_i)]dxdydz + \iiint_{\Delta V} r_i dxdydz = \iiint_{\Delta V} \frac{\partial(n c_i)}{\partial t} dxdydz \tag{6.23}$$

The first term in these two equations represent the flux-in or flux-out from boundaries of the control volume, the second term is the source of flux within the control volume, and the third term is the change in storage. In words, the flux-in from boundaries plus the flux generated within the control volume are equal to the storage change. These equations can be discretized by both finite-element and finite-difference methods. Unlike the traditional finite-element method, the control-volume finite-element method maintains the mass balance for each node instead of mass balance for the entire simulation domain. The mass balance at each node is calculated by summing mass fluxes from adjacent elements. Details on the method for solving equations (6.22) and (6.23) can be found in Zhang (1995).

Kinetic Reactions

A predictor-corrector procedure was applied by Zysset *et al*. (1994) for solving kinetic reaction equations. The method was implemented by separating reaction rates into production

rates and first-order loss rates.

$$r_i = \xi_i - \vartheta_i c_i \quad i=1, \ldots, N_{sp} \tag{6.24}$$

where ξ_i and ϑ_i are production and loss rates, respectively, and are non-linear functions of all species, and N_{sp} is the total number of reactive species. The reaction equation of a species is said to be stiff if

$$\Delta t^0 \vartheta > 1 \tag{6.25}$$

where Δt^0 is the time step size in the integration of equation (6.22) (Zysett *et al*., 1994). The predictor-corrector procedure is a very robust algorithm in terms of convergence. However, the computation is very intensive because the time step size Δt^0 is constrained by

$$\Delta t^0 = \alpha \min\left|c_i / r_i\right| \tag{6.26}$$

where α is a scale factor (estimated as $1x10^{-3}$ by Zysset *et al*., 1994). For a small value of $|c_i/r_i|$, an extremely tiny time step is required. Our test problems indicate that such a small time step is feasible for one-dimensional problems, but it took weeks on a Sun workstation to finish a run using the time step size. To overcome the stiff condition in equation (6.25) and improve the efficiency of reaction calculations, we implemented a variable time step procedure for solving equation (6.20), which is summarized as follows;

(1) Assign k=1 and $t_k = 0.0$. Here k is the time step index in the reaction calculations.

(2) Calculate first-order loss rate ϑ_i for each species and determine the maximum loss rate ϑ_{max} among the species.

(3) The time step size without causing the stiffness for the solution is

$$\Delta t_k = \frac{1}{\vartheta_{max}} \tag{6.27}$$

(4) The first-order loss reaction is calculated by

$$c_{i,m}^{R,t_k+\Delta t_k} = c_i^{R,t_k} e^{-\vartheta_{i,m}\Delta t_k} \tag{6.28}$$

where m is the index number for the *mth* iteration, and R is an index number for the reaction. Equation (6.28) ensures that no negative concentration is generated by the reaction step. The reaction rates $\vartheta_{i,m}$ are calculated by the average concentrations at the previous iteration of the current time step and at the previous time step.

(5) Calculation of the production rate is related to first-order loss rates by stoichiometric coefficients. The calculation is expressed as

$$c_{i,m}^{R,t_k+\Delta t_k} = c_i^{R,t_k} + \Delta c_{i,m}^{t_k+\Delta t_k} \tag{6.29}$$

The first term at left side of equation (6.29) is the concentration of species i at the current time step and the current iteration, and the first term on the right side of the equation (6.24) is the concentration of species i at the previous time step. The second term on the right side of equation (6.29) is a function of reactant changes in equation (6.28) so that one mole of reactant produces the corresponding number of moles of products, as determined by the stoichiometric coefficients in equations (6.3) through (6.7).

(5) Test the convergence of reaction solutions by

$$\left|c_{i,m+1}^{R,t_k+\Delta t_k} - c_{i,m}^{R,t_k+\Delta t_k}\right| < \varepsilon \left|c_{i,m+1}^{R,t_k+\Delta t_k}\right| \tag{6.30}$$

where ε is a small number defined as relative error. If the condition (6.30) is met, go to step (6); otherwise, go to step (4).

(6) Assign k=k+1 and $t_k = t_k + \Delta t_k$, and go to step (2) if $t_k < \Delta t$; otherwise stop calculations.

With such a modification, there was a significant speedup in the solution. Simulations were finished overnight with a Sun workstation or a powerful PC, as compared to weeks with a constant time step.

Simulation Results

Verification of Numerical Models

This section describes two verification tests with the ISCO3D code. We compare model results against a column experiment of NAPL dissolution to test the dissolution model. The column experiment data come from a study by Imhoff *et al*. (1994) who looked at the dissolution of NAPLs in saturated media. They packed washed silica sand in an aluminum cylinder with a diameter of 8.25 cm and a height of 7 cm. At the start of the experiment, the average TCE saturation was 0.16 throughout the column. During the experiment, a Darcy flux of 0.91 m/day was maintained to flush the DNAPL out of the sand column. We tested three empirical equations (Miller *et al*., 1990; Imhoff *et al*., 1994; and Powers *et al*., 1994) to match the TCE saturation at x = 31.5 mm (as Figure 6.5 in Imhoff *et al*., 1994), a measurement point that reflects a complete loss of TCE from the pores (Figure 6.1). All empirical equations generally matched the experimental saturation data. Miller's model matched the early-time part of the saturation curve better, but not the late-time part. Both Imhoff's and Powers' models matched the late-time part of the saturation curve better. In the verification exercise, the dissolution parameters for the three models are determined from respective references (Miller *et al*., 1990; Imhoff *et al*., 1994; and Powers *et al*., 1994) and the transport parameters are from Imhoff *et al*. (1994).

The second test compares our model results with an analytical solution that includes first-order decay reaction to test the coupling of mass transport and kinetic reactions. The purpose of this test is to verify that the operator-splitting approach works for a simple example. We used the USGS code,

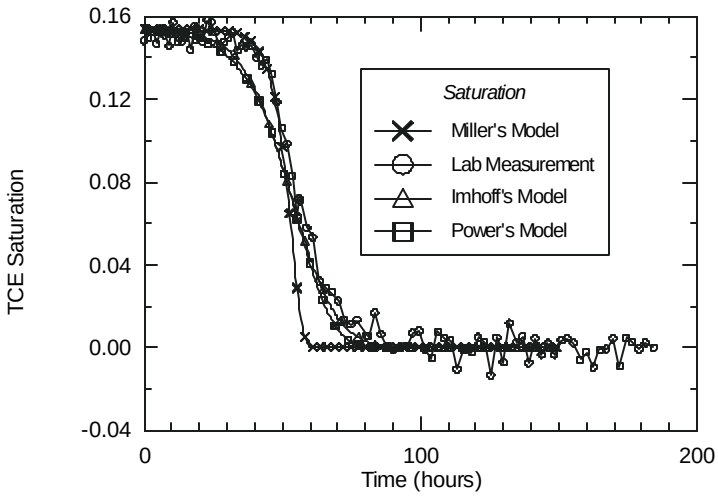

Figure 6.1. Test of the coupled transport and dissolution processes using three empirical dissolution models (Miller *et al*., 1990; Imhoff *et al*., 1994; and Powers *et al*., 1994).

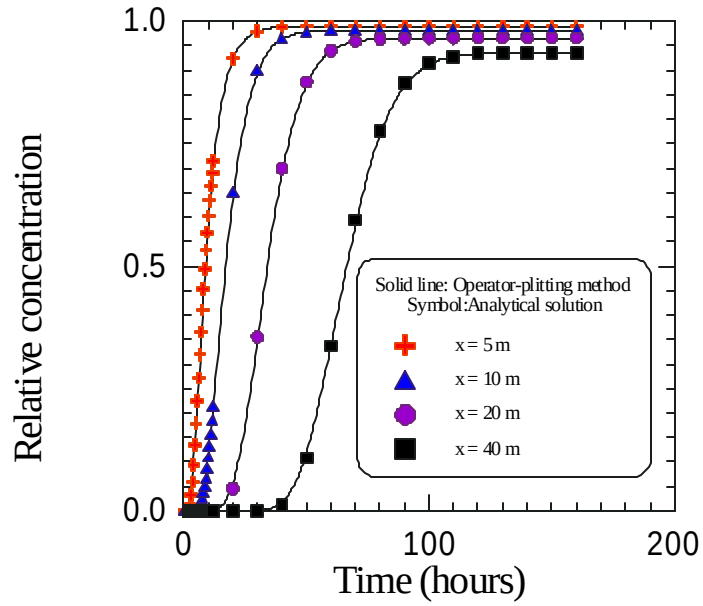

Figure 6.2. Verification of the operator-splitting approach using an analytical solution

FINITE (Wexler, 1992), to provide the analytical solution. A column, 40 m long, was set up with a third-type (variable flux) boundary condition at x = 0 with unit concentration. The other specified parameters were the linear ground water velocity (v) = 0.6 m/h, the effective diffusion coefficient (D_{eff}) = 0.6 m^2/h, and the decay constant (λ) = 0.001 h^{-1}. Breakthrough curves at x =5, 10, 20, and 40 m created using the operator-splitting approach matched exactly with the analytical solution (Figure 6.2).

General Description of Simulation Exercises

We demonstrate the application of the code using three examples. The first simulation attempted to reproduce column flushing experiments by Schnarr *et al.* (1998), using aquifer materials from the Canadian Forces Base Borden. The second set of simulations sought to match the Cl^- mass production rate in a field test designed as a proof-of-concept of source-zone flooding by MnO_4^- (Schnarr *et al*., 1998). The third set of simulations was based on a similar field-demonstration of $KMnO_4$ flooding at a DOE facility (West *et al*., 1997). In all of simulations, kinetic rates in Table 6.1 were used. In the following simulations, fitting parameters include dissolution rate constants α', β_1', and β_2', mass transfer coefficients k_f and k_r for the flowing-stagnant region model in the simulations of column experiments, and the quantity of the oxidizable aquifer materials (OAM). Other input parameters are kept constant during the try-and-error calibration process.

Various properties of chemical compounds and species relevant to these trials are listed in Table 6.3. The solubility of PCE varies from 150 to 200 mg/L (Callahan *et al*., 1979). A solubility value of 160 mg/L is selected in our study because the column experiments by Schnarr *et al.* (1998) exhibited a somewhat smaller effluent concentration (~100 mg/L) at the beginning of their experiments. The diffusion coefficient for all of the compounds and ion species was set to zero because

Table 6.3. Properties of Chemicals

Chemical species	Density (g/cm^3)	MW	K_{OC} (kg^{-1}/L^{-1})	Solubility (mg/L)
$KMnO_4$	2.703	118.94		60000
TCE	1.464	131.39	120	1277
PCE	1.623	165.83	468	150-200
CO_2		44.011		
Cl^-		35.457		
MnO_2(s)		86.94		
C		12.011		

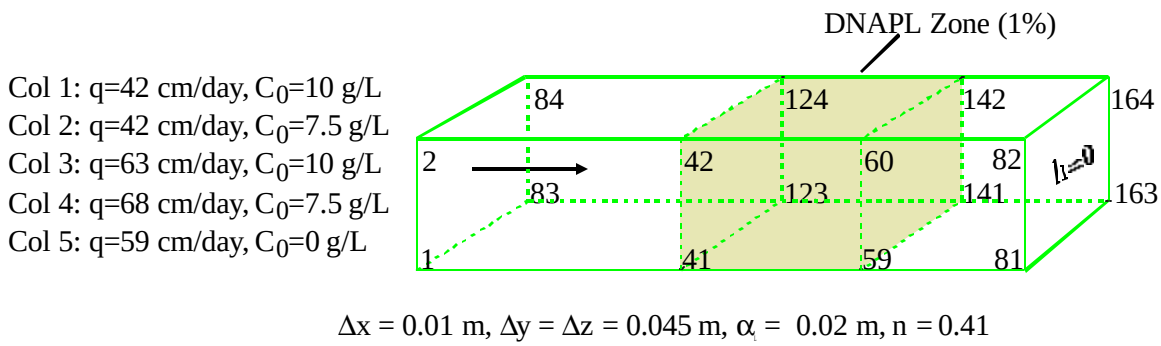

Figure 6.3. Model setup for the simulation of MnO_4^- oxidation of PCE in column experiments.

diffusion is likely negligible in all of the experiments as compared to the mechanical dispersion.

Simulation of Permanganate Treatment of PCE in Column Experiments

Schnarr *et al.* (1998) undertook column experiments to study PCE oxidation by $KMnO_4$. The glass columns (30 cm long, 5.2 cm ID) were packed with fine-grained sand from Canadian Forces Base Borden. This sand had a f_{oc} of 0.02%, and a porosity of 0.41. They flushed the 10 cm DNAPL zone placed near the top of the columns with a 10g/L $KMnO_4$ solution for 214 h, and then with deionized water to 680 hours. Because of the upward flow, the MnO_4^- oxidized organic matter and other reactive materials in the column, before it reached the NAPL zone. With time destruction of PCE in the aqueous phase enhanced the solubilization of the DNAPL.

Figure 6.3 shows the simulation domain and basic data for the five column experiments. The domain is discretized by 40 rectangular blocks with Δx = 0.01 m, and $\Delta y = \Delta z$ = 0.045m (Figure 6.3). To maintain a Peclet number of 2, a longitudinal dispersivity of 0.02 m was specified in the model. The measured porosity of 0.41 was assigned uniformly. A constant-head boundary condition was assumed at the end of column. The simulations utilized the experimental Darcy fluxes, which ranged from 42 to 68 cm/day (Figure 6.3). The initial concentrations of $KMnO_4$ ranged from 7.5 to 10 g/L w except for column 5. The initial PCE saturation was 1%.

Modeling the kinetic dissolution of pure-phase PCE requires various medium and NAPL parameters. The soil grain diameter d_{50} at the Borden site, 0.13 mm, was inferred from O'Hannesin (1981) and Ball *et al.* (1990). We defined a variable proportionality factor α' in the dissolution model (Eqn.13) to reflect the difference in dissolution rates in different column experiments, while keeping β_1'= 0.598 and β_2' = 0.938 constant (within the range of values in the Powers' model, 1994 and see Table 6.2). The difference in the dissolution rates in the five column experiments may be caused by the heterogeneity of aquifer materials, NAPL distribution, and variations in flow rates.

In each column experiment, there were three kinetic reactions of interest. A reaction rate constant from batch experiments (Table 6.1) (Yan and Schwartz, 1999) was used to describe oxidation of PCE by MnO_4^-. A large reaction rate constant of 450 $M^{-1}s^{-1}$ is assumed for reactions between oxidizable aquifer materials (OAM) and MnO_4^-. The approximate magnitude was estimated by the relative rate of migration of MnO_4^- as compared to the linear ground-water velocity.

The quantity of oxidizable material in the medium was a fitting parameter. Our simulations indicated that around 2.62 g/kg of soil materials, including natural organic carbon in the column provided the best match with the experimental results. This consumption of MnO_4^- by oxidizable compounds in the porous medium is evident in the delayed breakthrough curve of MnO_4^- in column experiment 3.

Figure 6.4 shows the breakthrough curves of MnO_4^- for column experiments 1 through 4. The simulated breakthrough curves for MnO_4^- are similar to the measured ones in terms of

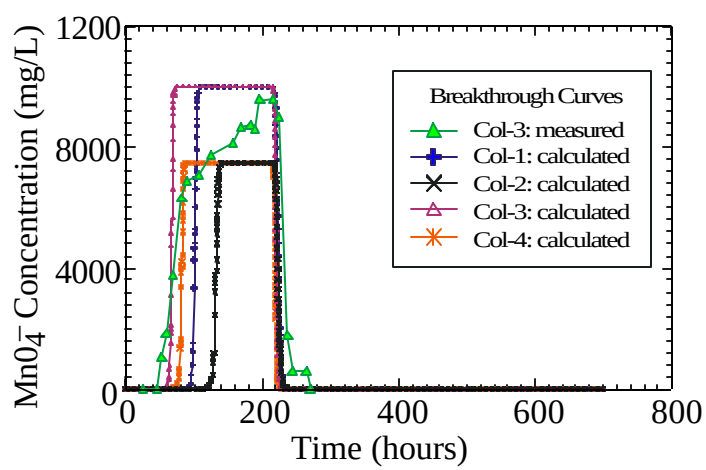

Figure 6.4. Calculated breakthrough curves of MnO_4^- for the column experiments 1 through 4 and the measured breakthrough curve for the column experiment 3.

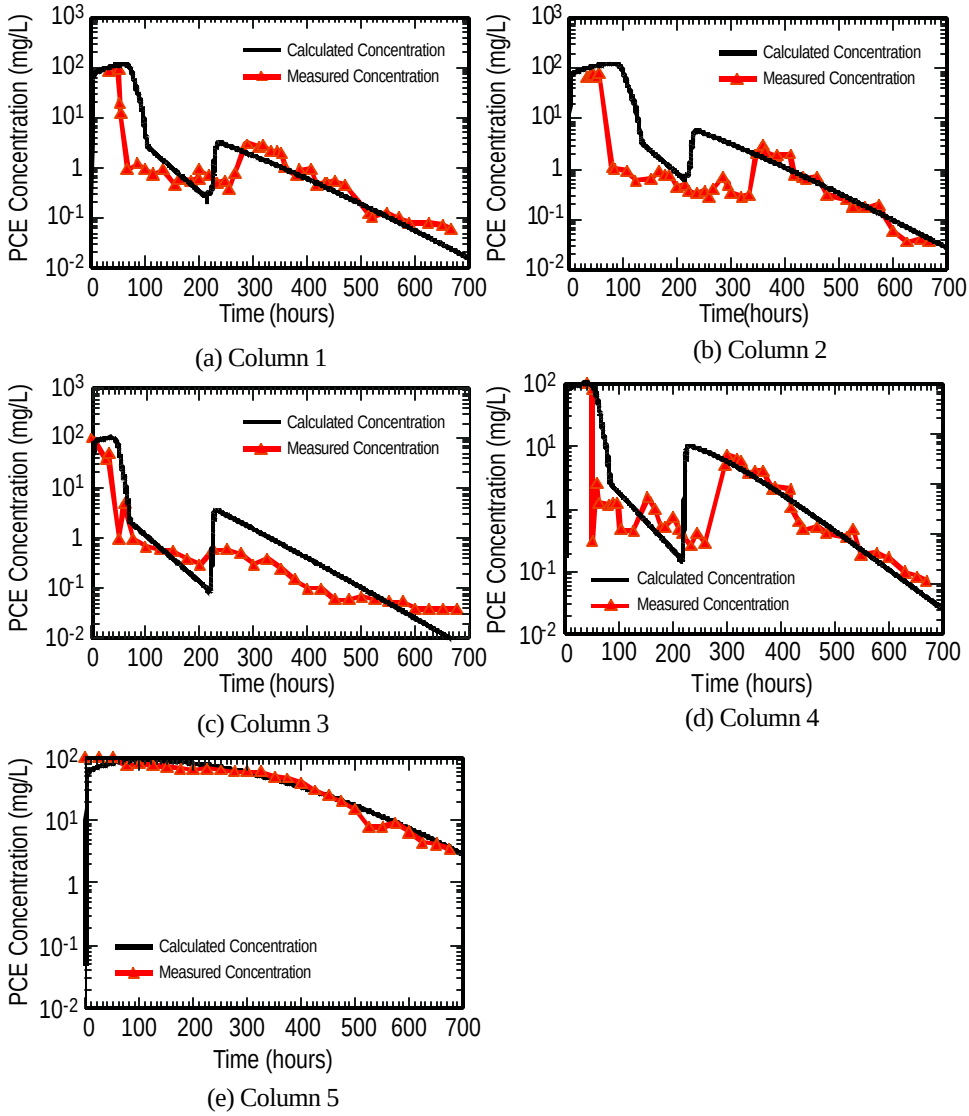

Figure 6.5. Simulated breakthrough curves for PCE for column experiments 1 through 5.

arrival times. However, as Figure 6.4 illustrates, the measured breakthrough curve for column 3 exhibits a lower concentration at early times. This may be due to preferential flow paths in the column along which the reactions could occur first. Diffusion carried reactive species from immobile regions in the column to flow paths as time progressed.

The simulated breakthrough curves for PCE are comparable to the measurements (Figures 6.5a through 6.5e). We were able to reproduce the dramatic concentration decrease in the aqueous phase once MnO_4^- was applied to the NAPL zone. When the MnO_4^- was replaced by water in the injection fluid the PCE concentrations were rebounded to a higher level. A difficulty in simulating PCE effluent concentrations in columns 1 through 4 is that a non-zero PCE concentration was observed when MnO_4^- effluent concentration approached its injection concentration. This result was not expected because MnO_4^- with large concentration (mg/L) should be able to oxidize PCE completely. There are several possible

Table 6.4. Kinetic reaction rate constants

Column No.	α	$k_f (s^{-1})$	$k_r (s^{-1})$
1	6365	$1x10^{-4}$	$6x10^{-6}$
2	9547	$1x10^{-4}$	$6x10^{-6}$
3	3182	$1x10^{-4}$	$6x10^{-6}$
4	2228	$1x10^{-4}$	$6x10^{-6}$
5	1273	$1x10^{-4}$	$6x10^{-6}$

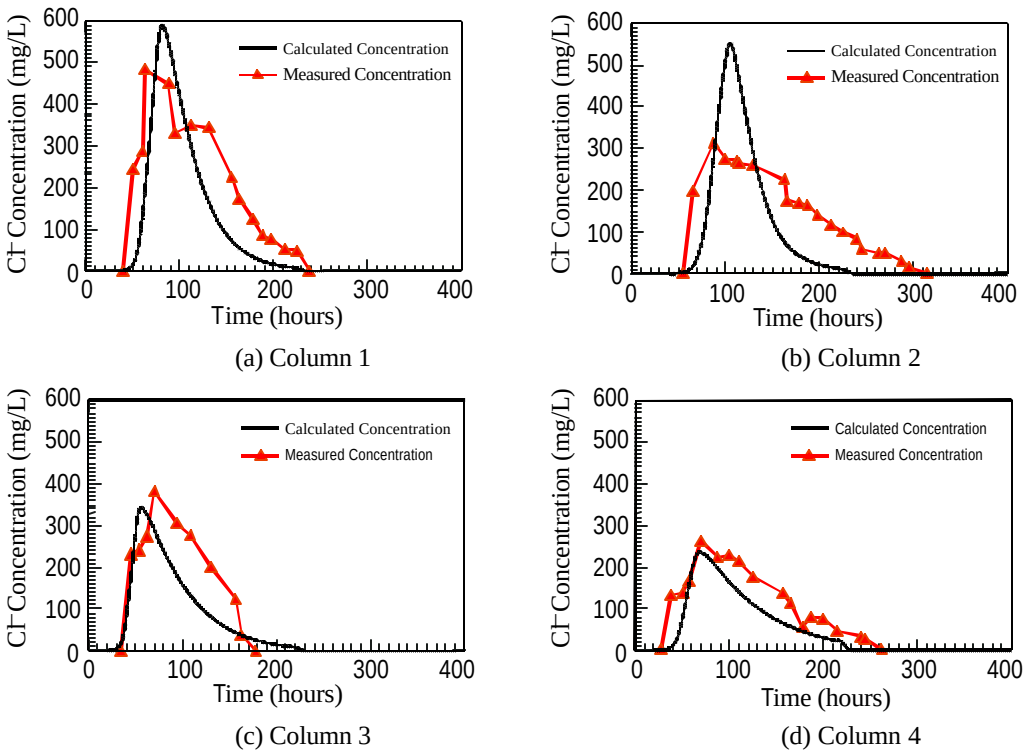

Figure 6.6. Simulated breakthrough curves for Cl^- for column experiments 1 through 4.

explanations for why this behavior occurred. With the data we have available from the column experiments it is not possible to interpret these results unambiguously. The presence of PCE might be caused by the kinetic sorption of PCE on the surface of the aquifer materials or more likely, preferential flow paths within the column. In effect, local scale heterogeneities in PCE distribution would provide zones that are not effectively being swept by the MnO_4^-. Mathematically, this process can be represented by the kinetic sorption/mass transfer model expressed by equation (6.7). Forward reaction rate constant k_f is the rate of mass transfer from a flowing region to a stagnant region. Reverse reaction rate constant k_r is the rate of mass transfer from a stagnant region to a flowing region. Table 6.4 lists the best-matched dissolution and mass transfer coefficients for the five column experiments. Clearly, there remains some uncertainty in the actual interpretation of the results of the column experiments that could not be resolved in our analysis.

The basic characteristics of the breakthrough curves of Cl^- were also simulated reasonably well (Figure 6.6) although there were differences between the measured and the calculated breakthrough curves.

Simulations of MnO_4^- Flooding in a Three-dimensional Test Cell Experiment

The next demonstration is based on a field-scale

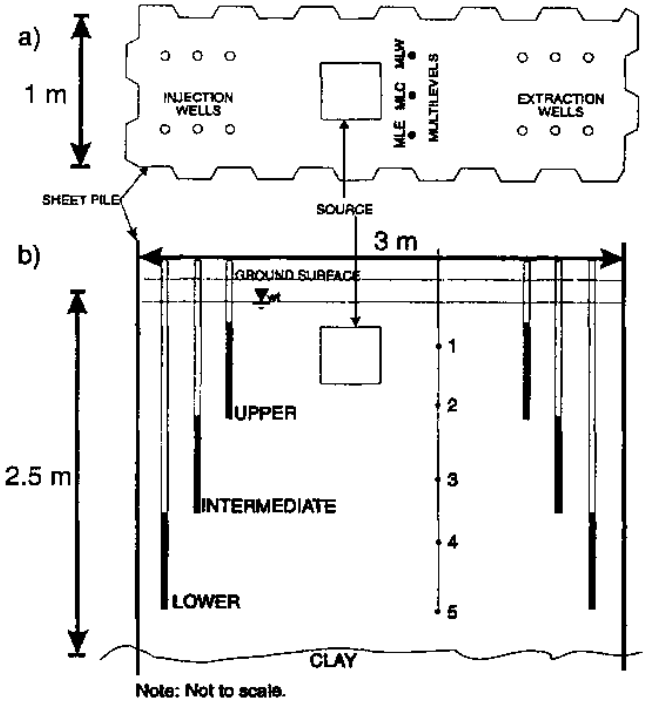

Figure 6.7. Basic setup for a field test cell at the CFB Borden site (Scharr *et al*, 1998).

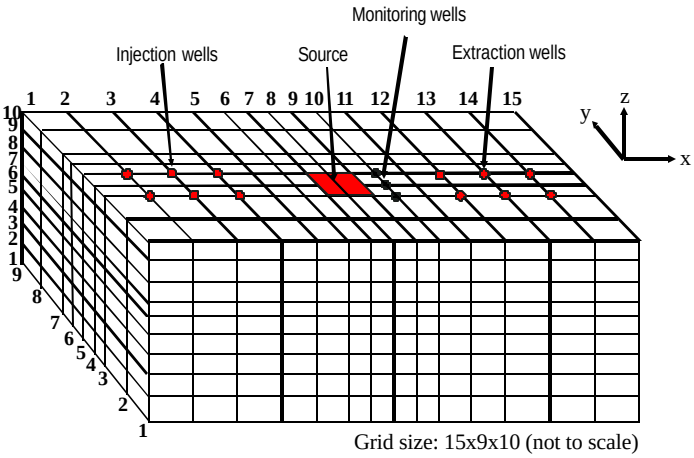

Figure 6.8. A three-dimensional model of the injection and extraction system in the Borden test cell

experiment at CFB Borden that demonstrated the potential of MnO_4^- flooding for removing pure-phase PCE (Schnarr *et al.*, 1998). The model conceptualization of the field experiment cell is shown in Figure 6.7. The experimental cell was 3 m in length, 1 m in width, and 2.5 m in height. We only simulated their first experiment where a PCE source at 8% saturation was emplaced in a zone of 0.3m x 0.3m x0.35m. Flow across the cell was maintained through a system of injection and withdrawal wells. In the simulation, we simulated this condition by maintaining constant heads in the six injection wells and by pumping the other six wells. The total extraction rate was 100 L/day from the beginning of the experiment to 50 days, and 50 L/day afterward to 180 days. Flooding with a MnO_4^- solution at 10 g/L continued over the first 120 days. Water was injected from 120 to 180 days. In the simulation, we used three stress periods (0 to 50 days for stress period 1, 50 to 120 days for stress period 2, and 120 to 180 days for stress period 3) to account for the variable mass loading and extraction rates during the experiment.

The complexity of this system requires a three-dimensional model (Figure 6.8). The simulation grid consists of 15 columns in the x direction, 9 slices in the y direction, and 10 rows in the z direction. Grid intervals range from 0.16 to 0.28 m in the x direction, 0.125 m in the y direction, and 0.175 to 0.5 m in the z direction. A horizontal hydraulic conductivity of 8.2 $x10^{-3}$ m/s and a vertical hydraulic conductivity of 6.3 $x10^{-3}$ m/s (Sudicky, 1986) were specified uniformly in the entire simulation domain. Longitudinal and transverse dispersivities of the aquifer material are 0.36 and 0.039 m (Freyberg, 1986), respectively. No flow boundary conditions were assumed on six sides of the domain except at wells. Other transport and reaction parameters are the same as that in the previous one-dimensional column simulations, except for 1.05 g/kg of soil materials reacting with MnO_4^-, and a dissolution rate constant $\alpha = 434$. There were no measurements for these two parameters in the original field experiment. Their values were established through calibration

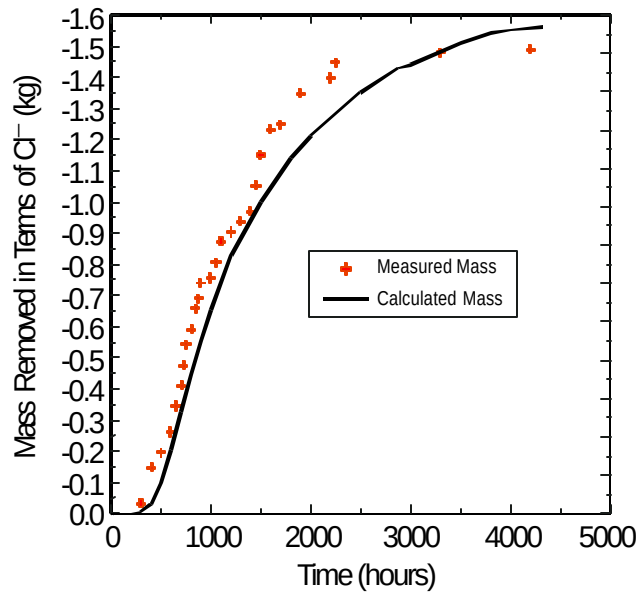

Figure 6.9. Simulated and measured mass removal rates in terms of Cl^- for the Borden test cell.

using patterns of Cl^- production. We suspect that the difference in flow heterogeneity between the column and the field materials and preferential flow paths may result in different reactivity and dissolution behaviors between one-dimensional and three-dimensional experiments.

Simulated mass removal rate in terms of Cl^- was compared with measurements (Figure 6.9). The two results exhibit a relatively close match after trial and error adjustment of reaction parameters. Interestingly, the mass removal rate could not be simulated without accounting for MnO_4^- oxidation of the aquifer materials. Thus, for both column and field cell experiments, simulations indicated that a major factor affecting the transport of the MnO_4^- front is the quantity of reactive materials existing in an aquifer. Column experiments by Drescher *et al.* (1998), which used materials from the Tyndall Air Force Base, Florida, showed that over 90% of MnO_4^- was consumed in the oxidation of the aquifer materials. It is therefore very important to implement column experiments to determine the extent of reaction between the aquifer materials and MnO_4^- before implementing a field experiment.

Simulation of A Field-Scale Experiment at a DOE Facility

A field-scale experiment of MnO_4^- oxidation of TCE was performed at the Department of Energy Portsmouth Gaseous Diffusion Plant (PORTS) in Ohio by researchers from Oak Ridge National Laboratory (ORNL) (West *et al.*, 1997). The field test involved injecting MnO_4^- in one horizontal well and extracting fluid in other horizontal well about 27 m up-gradient of the injection well (Figure 6.10). In this experiment, the MnO_4^- was recirculated, with provisions to "top up" MnO_4^- in the treatment fluid before reinjection.

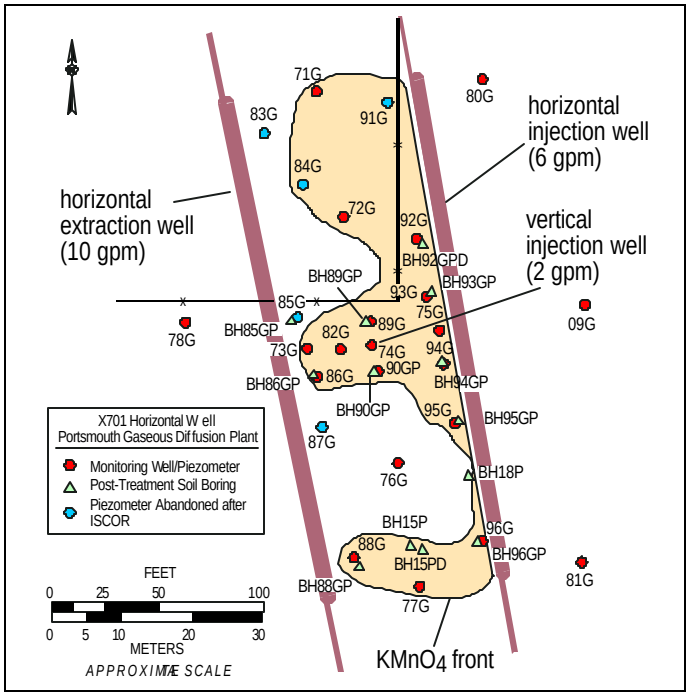

Figure 6.10. A field-scale experiment of permanganate oxidation of TCE at the Department of Energy Portsmouth Gaseous Diffusion Plant (PORTS) (West et al., 1997).

There are four major geological units of interest at the test area at Portsmouth (X701-B). The upper unit, the Minford silt and clay, has an average thickness of 7.5 m. The zone targeted for treatment is the Gallia sand and gravel with an average thickness of 1.5 m. Deeper units include the 4 m thick Sunbury shale, and the 15 m thick Berea Sandstone. Circulation of the injected fluid between the two parallel horizontal wells in the Gallia formation is facilitated by the relatively high hydraulic conductivity. However, the 27 m x 61 m zone between the two horizontal wells is heterogeneous in terms of hydraulic conductivity.

In the experiment, there was preferential flow of the MnO_4^- near the ends of the injection well (Figure 6.10). There was difficulty in the experiment in maintaining a constant injection/withdrawal rate of 10 gpm for both the injection and extraction wells. The injection rate was reduced to 6 gpm. MnO_4^- was also added through a vertical well at the center of the treatment zone to improve the efficiency of flooding. A total of 10,740 kg of $KMnO_4$ was injected between July 26 and August 27, 1997 through the horizontal well. In addition, 1960 kg of $KMnO_4$ was delivered using the vertical well (74G injected at 2 gpm) between August 20, 1997 and August 28, 1997. There was a significant reduction in the TCE concentration in the ground-water as the experiment continued.

Mahinthakumar and West (1997) simulated the migration front of MnO_4^- for the experiment. However, they did not explicitly consider the various chemical reactions taking place. In this study, simulations were aimed at not only providing the distribution of MnO_4^- but also the reactions among the different chemical species. We restricted our model to the Gallia formation because the injected fluids moved primarily through this higher permeability unit.

A two-dimensional model of 51x51 nodes was constructed to represent the treatment zone and its vicinity (Figure 6.11). The simulation grid was designed with relatively small node spacings inside the test region (Δx = 1m, and Δy = 2 m) and relatively large spacings outside (maximum Δx = 6 m, and maximum Δy = 7.5 m). The thickness of the simulation domain is the same as the Gallia formation (Δz = 1.5 m). The flow from the horizontal injection well to the Gallia was not uniformly distributed along the wellbore. As noted by West *et al.* (1997) and Korte *et al.* (1997), aquifer heterogeneity near the well, clogging of the well, or a pressure drop along the well screen may have contributed the variable flooding of the zone between the wells. Without additional data, we could not determine the exact cause of this pattern of flooding. To simplify the model

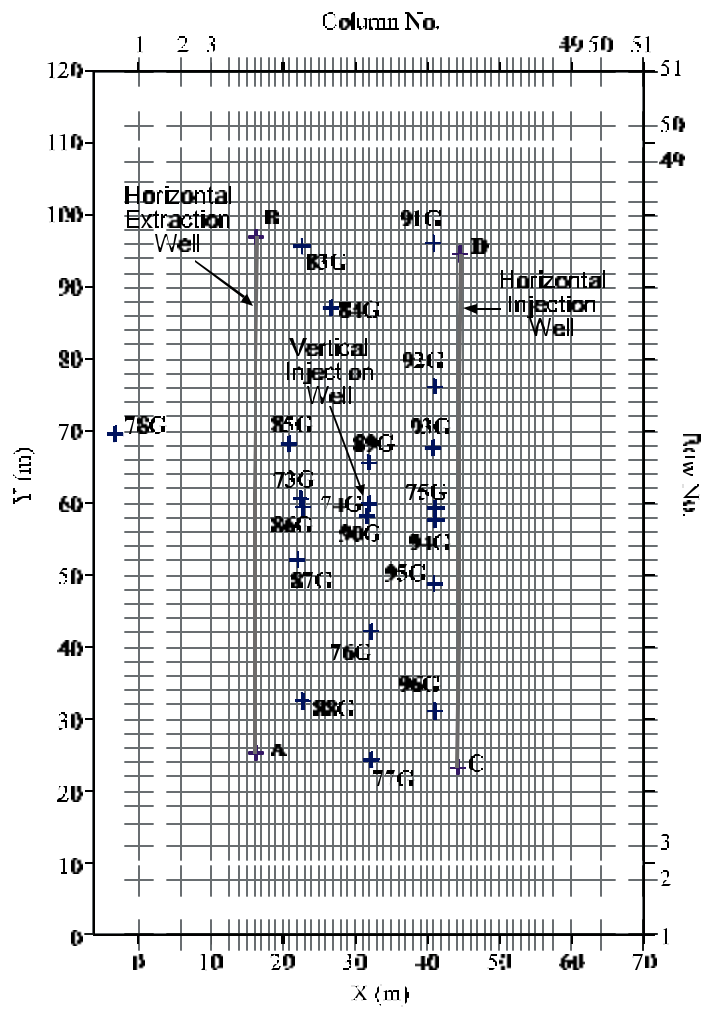

Figure 6.11. A two-dimensional model of 51x51 nodes representing the treatment zone and vicinity at the PORTS experiment site.

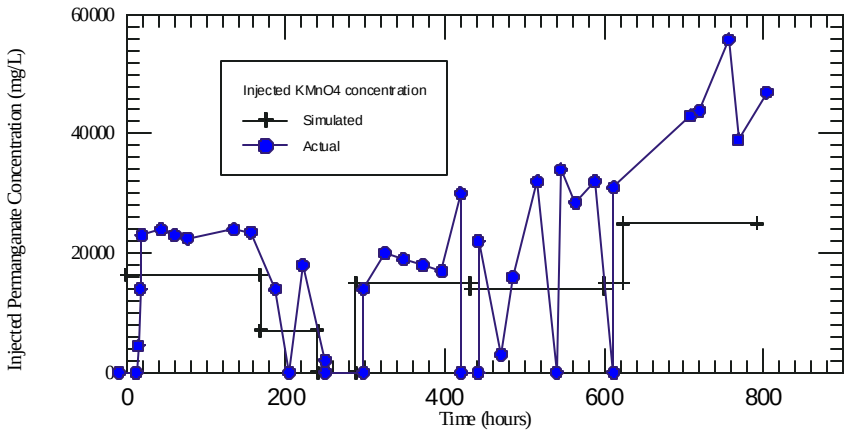

(a)

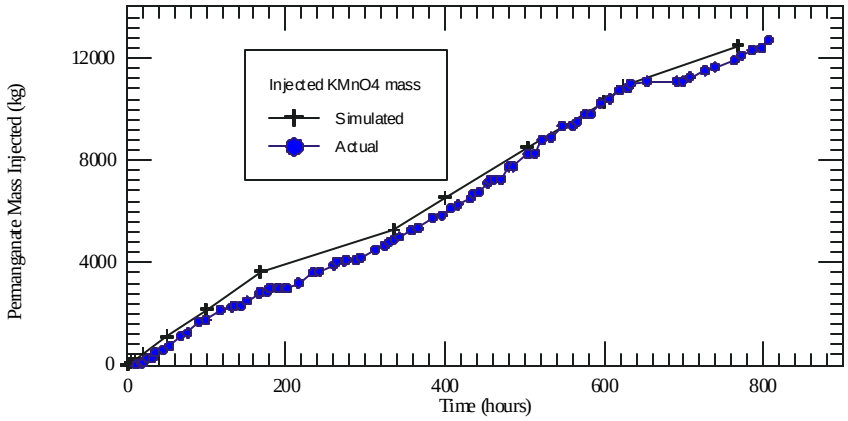

(b)

Figure 6.12. Inject permanganate mass. (a) Simulated and actual permanganate injection concentration in the horizontal injection well and the well 74G; (b) Simulated and actual accumulative injection mass.

setup, we adjusted flow rates along the well to provide the observed pattern of MnO_4^- flooding, while keeping the hydraulic conductivity constant. The MnO_4^- concentration used as input data to the model for the horizontal injection well and the well 74G approximated the actual pattern of loading (Figure 6.12a). The MnO_4^- concentration was constrained by recorded information on the mass rate of loading provided by a fluid injection rate of 6 gpm in the horizontal well and the 2 gpm in the vertical well. Injection mass in the simulations is specified as that in the field experiment (Figure 6.12b).

A mean hydraulic conductivity of 35 m/day is assumed in the entire simulation domain. Values of longitudinal and transverse dispersivity are selected as 5.0 and 0.5 m, respectively, to ensure a Peclet number less 2. The mean porosity of the Gallia is 0.2 as reported by Beard and Anderson (1996). A small regional horizontal gradient of 1.43×10^{-6} was imposed in the simulation region to provide for an ambient flow, although no hydraulic head measurements were reported in the test region by West *et al.* (1997).

The first task of this simulation exercise was to match approximately the observed MnO_4^- distribution through time. We selected three times (7 days, 32 days, and 120 days) following the start of MnO_4^- injection for this comparison. The initial concentration of TCE (Figure 6.14a) was from West *et al.* (1997). At time = 7 days, MnO_4^- was localized around the ends of the horizontal injection well (Figure 6.13a). At time = 32 days, note how the flooded zone expanded, and the center of the test region was flooded by MnO_4^- injected through well 74G (Figure 6.13b). Following the cessation of injection, unreacted MnO_4^- still remained in the aquifer for a period of time (Figure 6.13c). This residual MnO_4^- may be helpful for a while in oxidizing TCE in the aqueous phase, which likely was continuing to diffuse into the aquifer from zones above and below.

The simulation indicates that dissolved TCE concentrations were significantly reduced, where the MnO_4^- was delivered, as compared to the initial TCE concentration (Figure 6.14a). At time = 7 days, the contour line of 0.005 mg/L TCE (drinking water standard) is located near the horizontal injection well (Figure 6.14b). After 32 days, the zone of 0.005 mg/L or

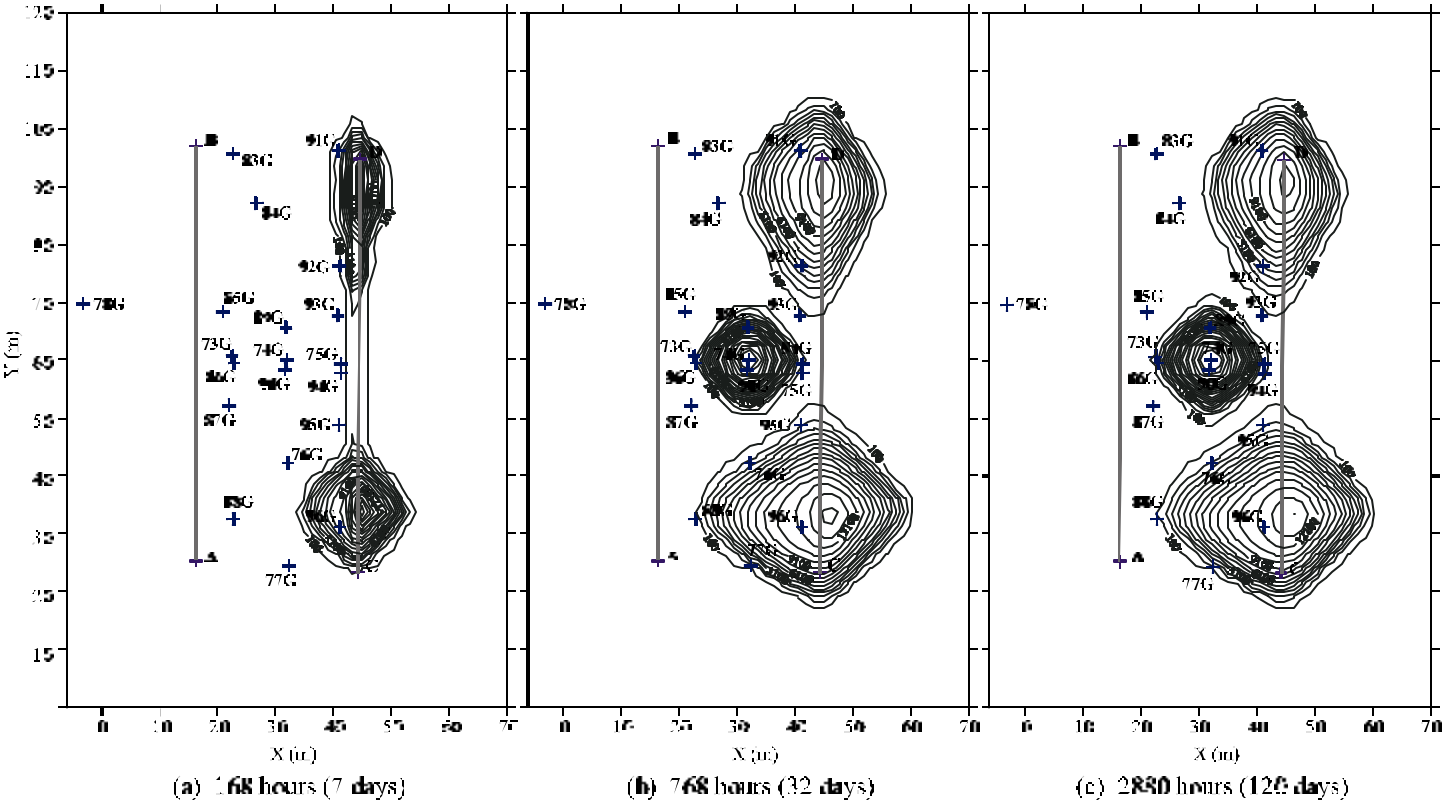

Figure 6.13. Simulated permanganate distribution. (a) Time = 7 days; (b) Time = 32 days; (c) Time = 120 days.

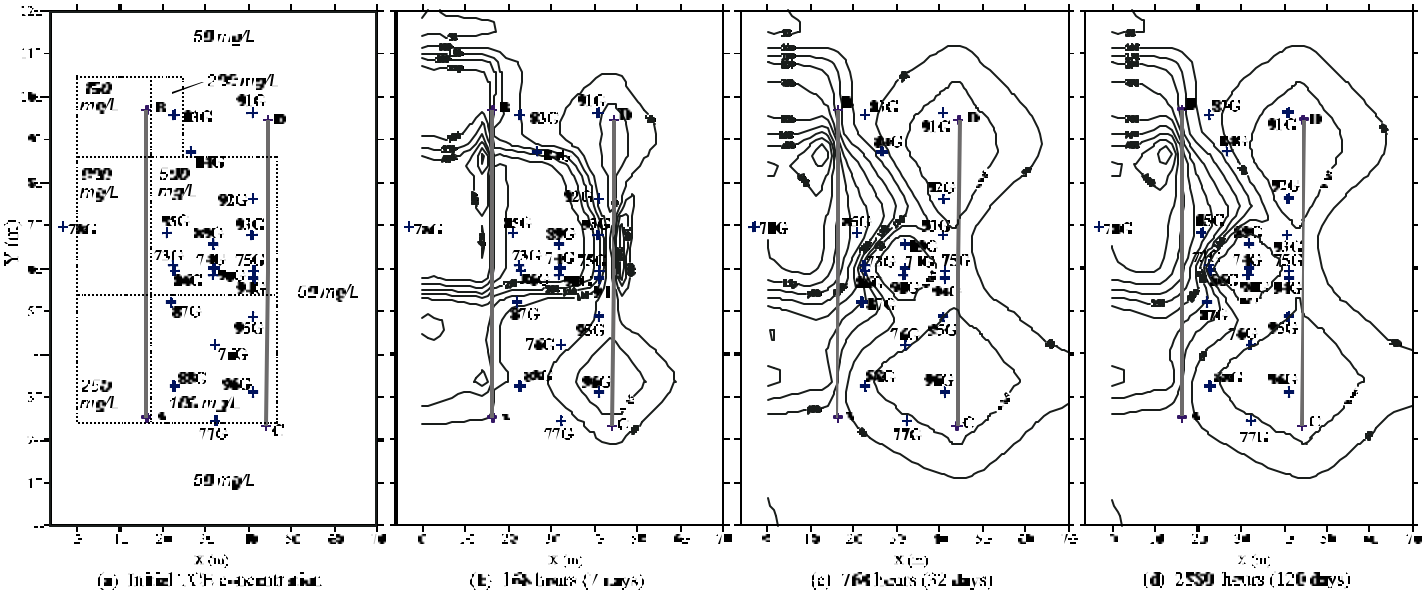

Figure 6.14. Simulated TCE distribution. (a) Time = 7 days; (b) Time = 32 days; (c) Time = 120 days.

less TCE concentration expanded outward significantly (Figure 6.14c). After this time (e.g., 120 days; Figure 6.14d), there is relatively little enlargement of the treated zone because the zone flooded by MnO_4^- didn't expand very much.

A detailed match of simulated and measured MnO_4^- distributions is impossible due to the lack of detailed hydraulic head measurement and the experimental determination of reactions between the MnO_4^- and the oxidizable aquifer materials (mainly organic carbon content). The present simulation suggests that 172 mg/kg of aquifer materials has been oxidized. Further sensitivity study indicates that the amount of oxidizable aquifer materials in the aquifer may significantly affect the transformation of TCE into non-harmful products (Figure 6.15). The area within which the TCE concentration is less than 0.005 mg/L is decreased as the amount of oxidizable aquifer materials is increased from 43 mg/kg to 430 mg/kg.

Concluding Remarks

A simulation and design tool was developed to model a remediation scheme that is based on the oxidation of chlorinated compounds by MnO_4^-. The computer code can simulate coupled processes including the dissolution of NAPLs; the chemical reactions among permanganate, dissolved chlorinated compounds, and aquifer materials; and the mass transport in three dimensions. We demonstrated the application of this code to a series of column experiments (Schnarr *et al*., 1998), one small field experiment (Schnarr *et al*., 1998), and a larger-scale field demonstration of source zone flushing (West *et al*., 1998). The success in generally matching this variety of experiments provides some initial confirmation that the code has been able to capture the essential physics and chemistry of the processes involved. The computer simulations, together with column, test cell, and field experiments also suggest that the proper determination of NAPL saturation, aqueous concentration of chlorinated compounds, and the reactivity between aquifer material and MnO_4^- are critical to a successful chemical oxidization design and field operation. This study and previous work also indicate that oxidization of chlorinated compounds is probably most efficient at a low NAPL saturation. The chemical reaction between the chlorinated compounds and MnO_4^- occurs in dissolved phase, but the dissolution of NAPLs is rate-limited. Our group is presently working to devise new approaches to accelerate the rate of oxidation.

Clearly, there is more work to be done in the development of the modeling approach outlined in this paper. For example, the experimental work has showed that the production of $MnO_2(s)$ is significant in the oxidative treatment of chlorinated compounds with permanganate. The $MnO_2(s)$ particles are transported and deposited as colloids during a remediation process. One of our current modeling initiatives is to study the effect of $MnO_2(s)$ on the efficiency of the oxidative scheme.

Acknowledgement

Funding of this study was supported by Department of Energy Environmental Management Science Program under grant #FG07-96ER14735. The data set for the verification of dissolution models was kindly provided by Dr. Paul Imhoff. Critical comments by Libby West, Carl Steefel, an anonymous reviewer, and an associate editor have improved the presentation of the materials in this study.

References

Ball, W.P., Ch. Buehler, T. C. Harmon, D.M. Mackay, and P. V. Roberts. Characterization of a sandy aquifer material at the grain scale. J. Contam. Hydrol., 5, 253-295, 1990.

Bear, J., Dynamics of fluids in porous media, American Elsevier, New York, 764 pp., 1972.

Beard, T. C., and F.J. Anderson, 3-D multiphase modeling of DNAPL TCE at the DOE Portsmouth Gaseous Diffusion Plant, Piketon, Ohio. Proceedings of ModelCARE 96 Poster Papers, International Conference on Calibration and Reliability in Groundwater Modeling. Golden, Colorado USA, September 24-26, 31-40, 1996.

Callahan, N. W., M. W. Slimak, N. W. Gabel, I. P. May, C. F. Fowler, J. R. Freed, P. Jennings, R. L. Durfee, F. C. Whitmore, B. Maestri, W. R. Mabey, B. R. Holt, and C. Gould, Water-related environmental fate of 129 priority pollutants, U. S. Environmental Protection Agency, Washington, D.C., 1979.

Colthurst, J. M., and P. C. Singer, Removing trihalomethane precursors by permanganate oxidation and manganese dioxide adsorption, Journal AWWA, 74, 78-83, 1982.

Drescher, E., A. Gavaskar, B. M. Sass, L. J. Cumming, M. J. Drescher, and T. K. J. Williamson, Batch and column testing to evaluate chemical oxidization of DNAPL source zones, Proceedings of The First International Conference on Remediation of Chlorinated and Recalcitrant Compounds, Vol. C1-5: Physical, Chemical, Thermal Technologies, Monterey, California, May 18-21, 425-432, 1998.

Freyberg, D. L. A natural gradient experiment on solute transport in a sand aquifer: 2. Spatial moments and the advective and dispersion of nonreactive tracers. Water Resour. Res., 22, 2031-2046, 1986.

Friedly, J., and J. Rubin, Solute transport with multiple equilibrium-controlled or kinetically controlled chemical reactions, Water Resour. Res., 28, 1935-1953, 1992.

Frind, E.O., Simulation of long-term transient density-dependent transport in groundwater, Adv. Water Resources, 5, 73-88, 1983.

Gates, D.D., R. L. Siegrist, and S. R. Cline, Chemical oxidation of volatile and semivolatile organic compounds in soil, Proceedings of 88th annual meeting and exhibition, San Antonio, 1995.

Huyakorn, P.S., and G.F. Pinder, Computational methods in subsurface flow, Academic Press, San Diego, Calif., 1983.

Imhoff, P. T., P. R. Jaffé, and G. F. Pinder, An experimental study of complete dissolution of a nonaqueous phase liquid in saturated porous media, Water Resour. Res., 30, 307-320, 1994.

Korte, N., M. Muck, P. Kearl, R. Siegrist, T. Houk, R. Schlosser, J. Zutman, Field evaluation of a horizontal well recirculation system for groundwater treatment: Field demonstration at X-701B Portsmouth Gaseous Diffusion Plant, Piketon, Ohio, Oak Ridge National Laboratory, Grand Junction, Colorado, 1997.

LaChance, J. C., S. Reisma, D. Mckay, and R. Baker, In situ oxidization of trichloroethene using potassium permanganate, Part 1: Theory and Design, Proceedings of The First International Conference on Remediation of Chlorinated and Recalcitrant Compounds, Vol. C1-5: Physical, Chemical, Thermal Technologies, Monterey, California, May 18-21, 397-402, 1998.

Letniowski, F. W., and P. A. Forsyth, A control volume finite element method for three-dimensional NAPL groundwater contamination, International Journal For Numerical Methods in Fluids, 13, 955-970, 1991.

Mahinthakumar, G, and O. R. West, High resolution numerical simulations in support of the ISCOR experiment at Portsmouth, Oak Ridge National Laboratory, Oak Ridge, Tennessee, 1997.

Mckay, D., A. Hewitt, S. Reisma, J. LaChance, and R. Baker, In situ oxidization of trichloroethene using potassium permanganate, Part 2: Pilot Study, Proceedings of The First International Conference on Remediation of Chlorinated and Recalcitrant Compounds, Vol. C1-5: Physical, Chemical, Thermal Technologies, Monterey, California, May 18-21, 377-382, 1998.

Miller, C. T., M. M. Poirier-McNeill, and A. S. Mayer, Dissolution of trapped nonaqueous phase liquids: Mass transfer characteristics, Water Resour. Res., 26, 2783-2796, 1990.

O'Hannesin, S. F. Spatial variability of grain-size parameters and hydraulic conductivity at a dispersion test site. Bachelor of environmental studies honors report. University of Waterloo, Waterloo, Ont., 46 p, 1981.

Pfannkuch, H.O., Determination of the Contaminant Source Strength form Mass Exchange Processes at the Petroleum-Ground-Water Interface in Shallow Aquifer Systems, in Petroleum Hydrocarbons and Organic Chemicals in Ground Water, National Water Well Assn., 111-129, 1984.

Powers, S. E., L. M. Abriola, and W. J. Weber, Jr., An experimental investigation of nonaqueous phase liquid dissolution in saturated subsurface systems: Steady state mass transfer rates, Water Resour. Res., 28, 2691-2706, 1992.

Powers, S. E., L. M. Abriola, and W. J. Weber, Jr., An experimental investigation of nonaqueous phase liquid dissolution in saturated subsurface systems: Transient mass transfer rates, Water Resour. Res., 30, 321-332, 1994.

Roberts, P. V., M. N. Goltz, and D. M. Mackay. A natural gradient experiment on solute transport in a sand aquifer: 3.Retardation estimates and mass balances for organic solutes, Water Resour. Res., 22, 2047-2058, 1986.

Schnarr, M., C. Truax, G. Farquhar, E. Hood, T. Gonullu, and B. Stickney, Laboratory and controlled field experiments using potassium permanganate to remediate trichloroethylene and perchloroethylene DNAPLs in porous media, Journal of Contaminant Hydrology, 29, 205-224, 1998.

Sleep, B., and J. Sykes, Modeling the transport of volatile organics in variably saturated media, Water Resour. Res., 25, 81-92, 1989.

Steefel, C. I., and K. T. B. MacQuarrie, Approaches to modeling of reactive transport in porous media, Reviews in Mineralogy, 34, 83-129, 1996.

Steward, R., Oxidation by permanganate, In Oxidation in organic chemistry, Wiberg, K. B., ed., Academic Press, New York, Part A, Chapter 1, 1-68, 1965.

Sudicky, E. A. A natural gradient experiment on solute transport in a sand aquifer: Spatial variability of hydraulic conductivity and its role in the dispersion process, Water Resour. Res., 22, 2069-2082, 1986.

Vella, P.A., and B. Veronda, Oxidation of trichloroethylene: comparison of potassium permanganate and Fenton's reagent, In Chemical oxidation technologies for the nineties, Eckenfelder, W.W., ed., Technomic publishing, Lancaster, Basel, 1992.

Valocchin and Malmstead, Accuracy of operator splitting for advection-dispersion-reaction problems, Water Resour. Res., 28, 1471-1476, 1992.

West, O. R., S. R. Cline, W. L. Holden, F. G. Gardner, B. M. Schlosser, J. E. Thate, D. A. Pickering, T. C. Houk, A full-scale demonstration of in situ chemical oxidation through recirculation at the X-701B site, Oak Ridge National Laboratory, Oak Ridge, TN, ORNL/TM-13556, 101 p., 1997.

Wexler, E.J., Analytical solutions for one-, two-, and three-dimensional solute transport in ground-water systems with uniform flow: U.S. Geological Survey Techniques of Water-Resources Investigations, book 3, chap. B7, 190 p, 1992.

Yan, Y. E., and F. W. Schwartz, Oxidative degradation and kinetics of chlorinated ethylenes by potassium permanganate, Journal of Contaminant Hydrology, 37, 343-365, 1999.

Yan, Y. E., and F. W. Schwartz, Oxidation of chlorinated solvents by permanganate, Proceedings of The First International Conference on Remediation of Chlorinated and Recalcitrant Compounds, Vol. C1-5: Physical, Chemical, Thermal Technologies, Monterey, California, May 18-21, 403-408, 1998.

Yeh, G. T., and V. S. Tripathi, A critical evaluation of recent developments in hydrgeochemical transport models of reactive multichemical components, Water Resour. Res., 25, 93-108, 1989.

Zhang, H., F.W. Schwartz, W.W. Wood, S. P. Garabedian, and D. R. LeBlanc, Simulation of variable-density flow and transport of reactive and nonreactive solutes during a tracer test at Cape Cod, Massachusetts, Water Resources Research, 34, 67-82, 1998.

Zhang, H., Simulations of multi-species contaminant transport in variable-density flow systems, Ph. D. dissertation, The Ohio State University, Columbus, Ohio, 1995.

Zysset, A., F. Stauffer, T. Dracos, Modeling of chemically reactive groundwater transport, Water Resources Research, 30, 2217-2228, 1994.

HOME BACK NEXT